

Spin fluctuations in a metallic antiferromagnet

Avinash Singh[†]

Department of Physics, Indian Institute of Technology Kanpur - 208016, India

The magnon energy and amplitude renormalization due to intraband particle-hole excitations are studied in a metallic antiferromagnet. The change in sign of the intraband contribution with ω results in significant differences between static and dynamical behaviours. For electron doping, while the coherent magnon peak loses spectral weight and is shifted to higher energy with doping, the low-energy incoherent part becomes increasingly prominent as it narrows in width and shifts to lower energy. Implications for spin dynamics in the electron doped cuprate $\text{Nd}_{2-x}\text{Ce}_x\text{CuO}_4$ are discussed. Due to an exact cancellation of two logarithmically divergent spin-fluctuation processes, the AF order parameter is unaffected to leading order. For hole doping, short wavelength transverse perturbations ($q > q^* \sim \sqrt{x}$) are found to be stable, implying short-range AF order with a spin correlation length $\xi/a \sim 1/\sqrt{x}$.

75.10.Lp, 75.30.Ds, 71.10.Fd

I. INTRODUCTION

Antiferromagnetism in the doped cuprates strongly depends on the type of doping. While the electron doped cuprate $\text{Nd}_{2-x}\text{Ce}_x\text{CuO}_4$ retains AF order up to a doping concentration of about 15%, [1–3] only 2% hole concentration destroys AF order in $\text{La}_{2-x}\text{Sr}_x\text{CuO}_4$.

The simplest microscopic description of this strong doping asymmetry emerges within the $t - t'$ Hubbard model, with nearest-neighbour (NN) and next-nearest-neighbour (NNN) hopping terms t and t' , respectively. For negative t' (as usually assumed for cuprates) and electron doping, the AF state is stable for a range of doping concentration, whereas the AF state becomes unstable with respect to transverse perturbations in the AF order for any finite hole doping. [4,5] Recently the magnetic phase diagram of the doped $t - t'$ Hubbard model has been obtained in the $t' - U$ space, showing the various regions of stability and instability with respect to both longitudinal and transverse perturbations in the AF order. [5]

The appropriate Hubbard model parameters for La_2CuO_4 , determined recently by fitting the spin-wave dispersion obtained from high resolution inelastic neutron scattering studies, [6–8] indicate that $U/t \sim 8$. From the additional fact that the critical electron doping concentration in $\text{Nd}_{2-x}\text{Ce}_x\text{CuO}_4$ is around 20%, the $t' - U$ phase diagram then yields $t'/t \sim 0.25$. [5] This value of t' falls in the range 0.15 to 0.5 estimated from band structure studies, photoemission data and neutron-scattering measurements of high- T_c and related materials. [9–12]

A stable AF state of the doped $t - t'$ Hubbard model provides a microscopic realization of a *metallic antiferromagnet*, in which the Fermi energy lies within a quasi-particle band. In this paper we will quantitatively study the interplay of spin fluctuations and particle-hole excitations in the metallic AF, focussing on the role of the intraband particle-hole excitations on the spin excitation spectrum, magnon renormalization, and spin-fluctuation correction to the AF order parameter. These results should be particularly relevant to the electron doped cuprate $\text{Nd}_{2-x}\text{Ce}_x\text{CuO}_4$, in which metallic conductivity resulting from electron doping suggests that the electrons are mobile, [13] and doping with Ce clearly reduces the spin-stiffness constant from the value in the undoped system. [3] Metallic antiferromagnetism has also been reported in $\kappa - (\text{BEDT} - \text{TTF})_2\text{X}$, [14] V_{2-x}O_3 , [15] and $\text{NiS}_{2-x}\text{Se}_x$. [16]

The metallic antiferromagnet is characterized by magnon decay into intraband particle-hole excitations, and the resulting magnon damping (Γ) was studied recently in the long wavelength limit ($q \ll 1$). [5] In terms of the Fermi circle radius $a = \sqrt{2\pi x}$ of the doping pockets formed around $(\pm\pi, 0)$ and $(0, \pm\pi)$, where x is the doping concentration, a new doping-dependent energy scale $4t'a$ was identified, the relative magnitude of which, in comparison with the magnon energy scale $\sqrt{2}J$, should essentially determine the spin excitation spectrum. The imaginary part of $\chi^0(\mathbf{q}, \omega)$ was found to vanish for $\omega > 4t'aq$, and increase linearly with ω for $\omega \ll 4t'aq$. This implies that the magnon spectrum should exhibit a sharp peak at $\omega \approx \sqrt{2}Jq$ for $\sqrt{2}J > 4t'a$ (low doping limit), and magnon broadening should appear with increasing doping when $\sqrt{2}J < 4t'a$.

In addition to the spin excitation spectrum for all q (section III), we will also study the quantum correction to sublattice magnetization (section IV), to determine whether long-range AF order survives in the metallic antiferromagnet when quantum spin fluctuations are included. At the one-loop level, the spin-flip process is accompanied by virtual magnon emission and absorption, and therefore we will also examine whether the magnon propagator (whose amplitude goes like $1/q$ in the AF insulator) is significantly renormalized due to the intraband particle-hole excitations (section II). The consequences of magnon renormalization on finite temperature spin dynamics and Néel temperature in electron doped cuprates are briefly discussed in section V.

We consider the $t - t'$ Hubbard model on a square lattice, with NN and NNN hopping terms t and t' connecting sites i to $i + \delta$ and $i + \kappa$, respectively:

$$H = -t \sum_{i,\delta,\sigma}^{NN} a_{i,\sigma}^\dagger a_{i+\delta,\sigma} - t' \sum_{i,\kappa,\sigma}^{NNN} a_{i,\sigma}^\dagger a_{i+\kappa,\sigma} + U \sum_i n_{i\uparrow} n_{i\downarrow}. \quad (1)$$

In the following we set $t = 1$. Since a particle-hole transformation maps the t' model with hole (electron) doping on the $-t'$ model with electron (hole) doping, the positive (negative) t' model and hole (electron) doping is appropriate to study for the electron-doped compound $\text{Nd}_{2-x}\text{Ce}_x\text{CuO}_4$, for which a negative t' is usually assumed.

II. MAGNON RENORMALIZATION

In this section we consider positive t' and hole doping, so that the results are appropriate for the electron-doped cuprates. We also consider the strong coupling limit for analytical simplicity. To study transverse spin fluctuations in the doped antiferromagnetic state we evaluate the time-ordered magnon propagator

$$\chi^{-+}(\mathbf{q}, \omega) = \int dt \sum_{\mathbf{r}_{ij}} e^{i(\omega t - \mathbf{q} \cdot \mathbf{r}_{ij})} \langle \Psi_G | T[S_i^-(t) S_j^+(0)] | \Psi_G \rangle \quad (2)$$

involving the spin-lowering and spin-raising operators S_i^- and S_j^+ at lattice sites i and j . In the random phase approximation (RPA), we have

$$\chi^{-+}(\mathbf{q}, \omega) = \frac{\chi^0(\mathbf{q}, \omega)}{1 - U\chi^0(\mathbf{q}, \omega)}, \quad (3)$$

where $\chi^0(\mathbf{q}, \omega)$ is the zeroth-order, antiparallel-spin particle-hole propagator, evaluated in the broken-symmetry, Hartree-Fock (HF) state of the metallic antiferromagnet, and involves both interband and intraband excitations. We examine the \mathbf{q}, ω dependence of $\chi^0(\mathbf{q}, \omega)$, which essentially determines the magnon energy and amplitude renormalization. We focus on the real part of $[\chi^0(\mathbf{q}, \omega)]$ in the underdoped limit, as its imaginary part was shown to vanish for $\omega > 4t'aq$ in the long wavelength limit. [5]

The HF-level description of the metallic AF state has been discussed earlier. [5] The NNN hopping term modifies only the AF-state quasiparticle energies $E_{\mathbf{k}}$, but not the quasiparticle amplitudes. We have $E_{\mathbf{k}}^\pm = \epsilon_{\mathbf{k}}' \pm \sqrt{\Delta^2 + \epsilon_{\mathbf{k}}'^2}$, for the upper and lower Hubbard bands, where $\epsilon_{\mathbf{k}} = -2t(\cos k_x + \cos k_y)$ and $\epsilon_{\mathbf{k}}' = -4t' \cos k_x \cos k_y$ are the free-fermion energies corresponding to the NN and NNN hopping terms. Here $2\Delta = mU$ in terms of the sublattice magnetization m .

In the two-sublattice basis (labelled by A and B), the intraband contributions to the diagonal and off-diagonal matrix elements of $[\chi^0(\mathbf{q}, \omega)]$ are obtained as:

$$\begin{aligned} [\chi^0(\mathbf{q}, \omega)]_{AA}^{\text{intra}} &= \frac{1}{4\Delta^2} \sum_{\mathbf{k}}' \left[\frac{\Delta_{\mathbf{q}}(\epsilon_{\mathbf{k}-\mathbf{q}}^2 + \epsilon_{\mathbf{k}}^2) - \omega(\epsilon_{\mathbf{k}-\mathbf{q}}^2 - \epsilon_{\mathbf{k}}^2)}{\Delta_{\mathbf{q}}^2 - \omega^2} \right] \\ [\chi^0(\mathbf{q}, \omega)]_{BB}^{\text{intra}} &= \frac{1}{4\Delta^2} \sum_{\mathbf{k}}' \left[\frac{\Delta_{\mathbf{q}}(\epsilon_{\mathbf{k}-\mathbf{q}}^2 + \epsilon_{\mathbf{k}}^2) + \omega(\epsilon_{\mathbf{k}-\mathbf{q}}^2 - \epsilon_{\mathbf{k}}^2)}{\Delta_{\mathbf{q}}^2 - \omega^2} \right] \\ [\chi^0(\mathbf{q}, \omega)]_{AB}^{\text{intra}} &= \frac{1}{4\Delta^2} \sum_{\mathbf{k}}' \left[\frac{\Delta_{\mathbf{q}}(2\epsilon_{\mathbf{k}}\epsilon_{\mathbf{k}-\mathbf{q}})}{\Delta_{\mathbf{q}}^2 - \omega^2} \right] = [\chi^0(\mathbf{q}, \omega)]_{BA}^{\text{intra}} \end{aligned} \quad (4)$$

where $\sum_{\mathbf{k}}'$ indicates that states \mathbf{k} are below the Fermi energy E_F , while states $\mathbf{k} - \mathbf{q}$ are above E_F , and $\Delta_{\mathbf{q}} \equiv E_{\mathbf{k}-\mathbf{q}}^\ominus - E_{\mathbf{k}}^\ominus$ is the intraband particle-hole energy difference in the lower Hubbard band.

The above three intraband contributions can be written, in units of (t^2/Δ^3) , as $(a_{\mathbf{q}} - b_{\mathbf{q}}\omega/2J)$, $(a_{\mathbf{q}} + b_{\mathbf{q}}\omega/2J)$, and $c_{\mathbf{q}}$, respectively. The dimensionless coefficients $a_{\mathbf{q}}, b_{\mathbf{q}}, c_{\mathbf{q}}$ are all functions of ω^2 and, for $\omega \neq 0$, vanish quadratically with q as $q \rightarrow 0$ due to phase space restriction. [5] However, for $\omega \propto q$ (near the magnon-mode energy), they all have well defined limits as $q \rightarrow 0$.

Including the interband contributions as well, which were studied earlier for finite doping up to order x^2 , [5] $[\chi^0(\mathbf{q}, \omega)]$ can be written as

$$\chi^0(\mathbf{q}, \omega) = \frac{1}{U} - \frac{t^2}{\Delta^3} \begin{bmatrix} 1 - a'_{\mathbf{q}} - a_{\mathbf{q}} + \tilde{\omega} & \gamma_{\mathbf{q}} - c_{\mathbf{q}} \\ \gamma_{\mathbf{q}} - c_{\mathbf{q}} & 1 - a'_{\mathbf{q}} - a_{\mathbf{q}} - \tilde{\omega} \end{bmatrix}. \quad (5)$$

The term $a'_{\mathbf{q}}$ represents modifications in the interband contribution due to NNN exchange energy $J' = 4t'^2/U$ and finite doping, and to first order in x , is given by

$$\begin{aligned} a'_{\mathbf{q}} &= \frac{J'}{J} \left(1 - \frac{\Delta x}{t'} \right) (1 - \gamma'_{\mathbf{q}}) \\ &+ x(\cos q_x - \cos q_y)^2 - \frac{2J'}{J} x(1 - \gamma'_{\mathbf{q}})^2, \end{aligned} \quad (6)$$

where $\gamma_{\mathbf{q}} = (\cos q_x + \cos q_y)/2$ and $\gamma'_{\mathbf{q}} = \cos q_x \cos q_y$. The scaled frequency $\tilde{\omega} = m^2(1 + b_{\mathbf{q}})(\omega/2J) \equiv f_{\mathbf{q}}(\omega/2J)$, where $m = 1 - x$, reflects the frequency-scale renormalization due to doping and intraband excitations.

Substituting $\chi^0(\mathbf{q}, \omega)$ from Eq. (5) in Eq. (3), the RPA-level magnon propagator is obtained as

$$\begin{aligned} \chi^{-+}(\mathbf{q}, \omega) &= -\frac{1}{2} \frac{m}{1 + b_{\mathbf{q}}} f_{\mathbf{q}}^{-1} \\ &\times \begin{bmatrix} (1 - a'_{\mathbf{q}} - a_{\mathbf{q}}) - \tilde{\omega} & -(\gamma_{\mathbf{q}} - c_{\mathbf{q}}) \\ -(\gamma_{\mathbf{q}} - c_{\mathbf{q}}) & (1 - a'_{\mathbf{q}} - a_{\mathbf{q}}) + \tilde{\omega} \end{bmatrix} \\ &\times \frac{2J}{\Omega_{\mathbf{q}}(\omega)} \left(\frac{1}{\omega - \Omega_{\mathbf{q}}(\omega)} - \frac{1}{\omega + \Omega_{\mathbf{q}}(\omega)} \right), \end{aligned} \quad (7)$$

where

$$\Omega_{\mathbf{q}}(\omega) = 2Jf_{\mathbf{q}}^{-1}[(1 - a'_{\mathbf{q}} - a_{\mathbf{q}})^2 - (\gamma_{\mathbf{q}} - c_{\mathbf{q}})^2]^{1/2} \quad (8)$$

is frequency dependent due to the intraband contribution, resulting in the magnon amplitude renormalization. The magnon-mode energies for momentum q are given by the poles at $\omega_{\mathbf{q}} = \pm\Omega_{\mathbf{q}}(\omega_{\mathbf{q}})$.

For $J \ll 8t'$, as in the strong coupling limit, the magnon renormalization due to $b_{\mathbf{q}}$ is negligible, and in the following we take the frequency-scale renormalization factor $f_{\mathbf{q}} = m^2(1 + b_{\mathbf{q}}) \approx 1$, for simplicity.

In the long-wavelength and low-doping limits ($q \ll 1, x \ll 1$) we have $\gamma_{\mathbf{q}} \approx 1 - q^2/4$, $\gamma'_{\mathbf{q}} \approx 1 - q^2/2$, and $a_{\mathbf{q}}, b_{\mathbf{q}}, c_{\mathbf{q}} \ll 1$. Substituting for $a'_{\mathbf{q}}$ from Eq. (6) in Eq. (8), the expression for $\Omega_{\mathbf{q}}(\omega)$ simplifies to

$$\Omega_{\mathbf{q}}(\omega) = \sqrt{2J}[\alpha_{\text{inter}} - \alpha_{\text{intra}}(\omega)]^{1/2}q \quad (9)$$

where the dimensionless quantities

$$\alpha_{\text{inter}} = 1 - (2J'/J)(1 - \Delta x/t') \quad (10)$$

$$\text{and } \alpha_{\text{intra}}(\omega) = 4(a_{\mathbf{q}} - c_{\mathbf{q}})/q^2 \quad (11)$$

were introduced earlier as coefficients of the q^2 term in the interband and intraband contributions to the transverse response eigenvalue in the context of the stability analysis of the doped AF state of the $t - t'$ Hubbard model. [5] From Eq. (4) which defines $a_{\mathbf{q}}, b_{\mathbf{q}}$, and $c_{\mathbf{q}}$, and substituting for $\epsilon_{\mathbf{k}-\mathbf{q}} - \epsilon_{\mathbf{k}} \approx 2tqa \cos \theta$, and the intraband particle-hole energy difference $E_{\mathbf{k}-\mathbf{q}}^{\ominus} - E_{\mathbf{k}}^{\ominus} \equiv \Delta_{\mathbf{q}} \approx 4t'qa \cos \theta$ in the limits $t' > Jx$ and $q \ll 1$, we obtain

$$\alpha_{\text{intra}}(\omega) = \frac{\Delta x}{t'} \int_{-\pi/2}^{\pi/2} \frac{d\theta}{\pi} \frac{\cos^4 \theta}{\cos^2 \theta - (\omega/4t'qa)^2}. \quad (12)$$

As $\alpha_{\text{intra}}(\omega)$ is a function of ω/q , it follows from Eq. (9) that the magnon-mode energy $\omega_{\mathbf{q}}$ is proportional to q , as in the AF insulator.

The change in sign of the intraband coefficient $\alpha_{\text{intra}}(\omega)$ at $\omega/4t'qa = 1$ (see Fig. 1) has interesting consequences on the doping dependence of the magnon-mode energy. In the static limit, $\alpha_{\text{intra}}(0) = \Delta x/2t'$ is positive, and the intraband contribution softens the magnon mode, eventually leading to the instability of the AF state when $\alpha_{\text{intra}} = \alpha_{\text{inter}}$. [5] However, for $\omega > 4t'qa$, the intraband coefficient α_{intra} is negative, implying that the intraband excitation actually stiffens the magnon-mode.

Therefore, for $\sqrt{2J} > 4t'a = 4t'\sqrt{2\pi x}$ (underdoped limit), the coherent magnon peak at $\omega_{\mathbf{q}} \approx \sqrt{2J}q$ is shifted to higher energy, this shift being proportional to x^2 in the small doping limit. With increasing doping, when $\sqrt{2J} < 4t'a$, the magnon peak is broadened due to damping and gets shifted to lower energy due to the change in sign of $\alpha_{\text{intra}}(\omega)$. As the magnon damping term goes as ω for $\omega \ll 4t'qa$, [5] the magnon peak significantly narrows down as it shifts to lower energies with doping.

Doping stiffens the magnon mode through the interband contribution as well, by suppressing the softening due to the J' -induced frustration. This is clearly seen from the expression for the interband coefficient α_{inter} in Eq. (10), which increases with x .

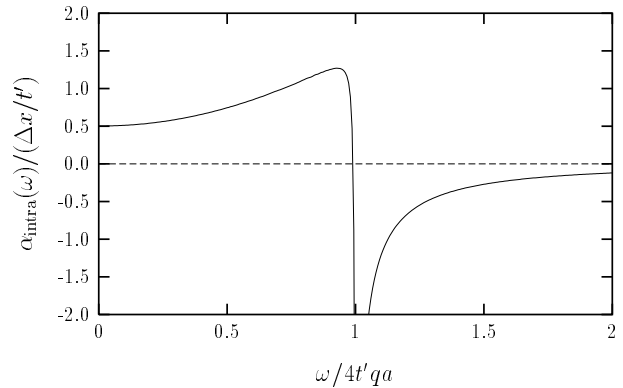


FIG. 1. The intraband coefficient $\alpha_{\text{intra}}(\omega)$ changes sign at $\omega = 4t'qa$, implying that the magnon-mode softening for $\omega_{\mathbf{q}} < 4t'qa$ changes into magnon-mode stiffening for $\omega_{\mathbf{q}} > 4t'qa$.

Turning now to the magnon amplitude renormalization, by expanding the frequency-dependent energy $\Omega_{\mathbf{q}}(\omega)$ near the mode energy $\omega_{\mathbf{q}}$, we obtain

$$\omega - \Omega_{\mathbf{q}}(\omega) \approx \left(1 - \left.\frac{\partial \Omega_{\mathbf{q}}}{\partial \omega}\right|_{\omega_{\mathbf{q}}}\right) (\omega - \omega_{\mathbf{q}}), \quad (13)$$

which yields the magnon renormalization factor

$$Z = \left(1 - \left.\frac{\partial \Omega_{\mathbf{q}}}{\partial \omega}\right|_{\omega_{\mathbf{q}}}\right)^{-1}. \quad (14)$$

From Eqs. (9) and (12), we obtain

$$\left.\frac{\partial \Omega_{\mathbf{q}}}{\partial \omega}\right|_{\omega_{\mathbf{q}}} = - \left(\frac{\sqrt{2J}}{4t'a}\right)^2 \frac{\Delta x}{t'} \int_{-\pi/2}^{\pi/2} \frac{d\theta}{\pi} \frac{\cos^4 \theta}{[\cos^2 \theta - (\omega_{\mathbf{q}}/4t'qa)^2]^2} \quad (15)$$

which is negative, and vanishes with the doping concentration as x^2 , through the x dependence of the integral. These consequences of doping, namely the stiffening of the magnon mode and reduction in the coherent spectral weight for low doping, changing into magnon softening and broadening with increasing doping, are confirmed in a numerical study of the magnon spectral function, as discussed below.

III. SPIN FLUCTUATION SPECTRUM

The spectrum of transverse spin fluctuations in the doped AF state, evaluated numerically from the imaginary part of the magnon propagator $\chi^{-+}(\mathbf{q}, \omega)$, is discussed in this section. In terms of the two complex eigenvalues $\lambda_n(\mathbf{q}, \omega)$ of the $\chi^0(\mathbf{q}, \omega)$ matrix, we obtain for the spin fluctuation spectral function $A_{\mathbf{q}}(\omega)$

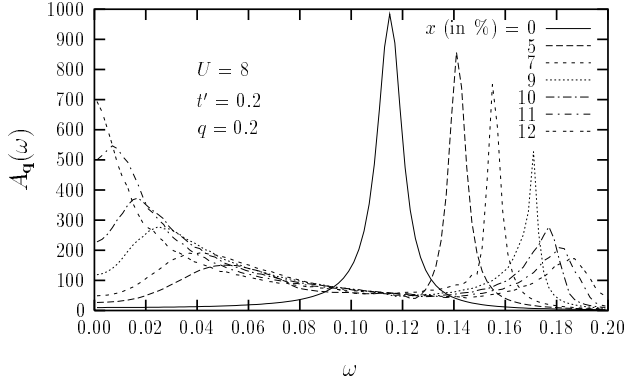


FIG. 2. The magnon spectral function $A_{\mathbf{q}}(\omega) = \text{Tr Im } \chi^{-+}(\mathbf{q}, \omega)$ for a long wavelength mode $\mathbf{q} = (0.2, 0)$, showing the shift of the coherent magnon peak to higher energy with doping, accompanied by a reduction of the magnon amplitude. With increasing doping the broad incoherent spectrum acquires strength and narrows into a peak which shifts down in energy.

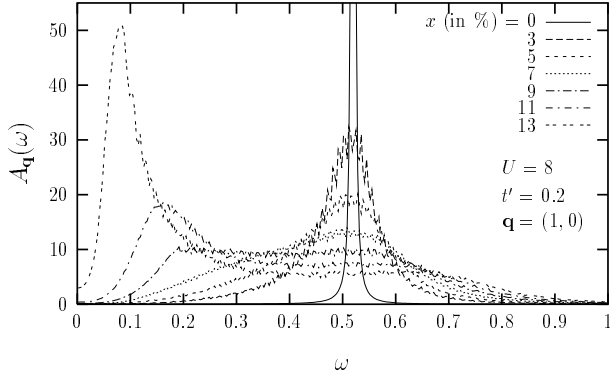


FIG. 3. For the short-wavelength mode $\mathbf{q} = (1, 0)$, the magnon peak broadens almost immediately with doping, with no change in the peak energy. With increasing doping, the magnon peak becomes strongly asymmetric, rapidly narrowing into a strong peak at low energy.

$$A_{\mathbf{q}}(\omega) = \text{Tr Im } \chi^{-+}(\mathbf{q}, \omega) = \sum_{n=1,2} \text{Im} \frac{\lambda_n(\mathbf{q}, \omega)}{1 - U\lambda_n(\mathbf{q}, \omega)}. \quad (16)$$

In the numerical evaluation of the $\chi^0(\mathbf{q}, \omega)$ matrix, we have taken a grid size $dk_x = dk_y = 0.01$ and an imaginary term $\eta = 0.001$ throughout. The spectral function $A_{\mathbf{q}}(\omega)$ has been recently studied for the AF insulator in the full U range from weak coupling to strong coupling, including contributions from both single-particle and collective (magnon) excitations. [17] In the following, we discuss the results in the context of cuprates, separately considering electron doping (positive t' and hole doping) and hole doping (negative t' and hole doping).

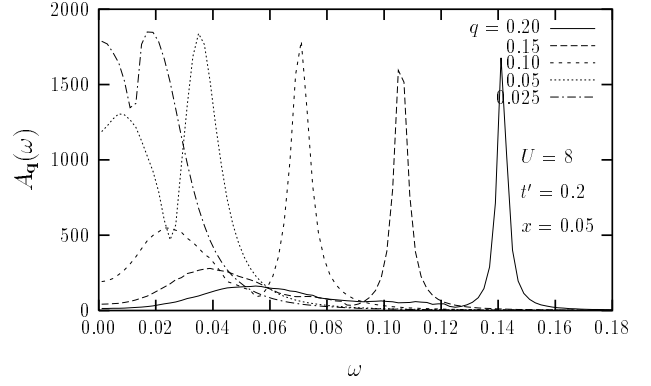


FIG. 4. For a fixed doping concentration, the magnon spectral function for different q shows a linear dependence of the coherent magnon peak energy $\omega_{\mathbf{q}}$ on q . With decreasing q the incoherent part is compressed into a narrow peak, which competes in strength with the coherent peak.

A. Electron doping

The results for $A_{\mathbf{q}}(\omega)$ are shown in Figs. 2-5, which confirm the characteristic features obtained in the magnon renormalization study of section II in the small q limit. With doping, the coherent magnon peak shifts to higher energy with decreasing amplitude (see Fig. 1). Simultaneously, the incoherent part of the magnon spectral function at low frequency progressively becomes narrower, shifts to lower energy and develops oscillator strength. The softening is due to the intraband contribution and the narrowing follows from the behaviour of $\text{Im } \chi^0(\mathbf{q}, \omega)$, which decreases with ω .

On the other hand, for short wavelength modes, the magnon peak is seen to broaden almost immediately with doping (see Fig. 3), with no change in the peak energy. A study of the imaginary part of $\chi^0(\mathbf{q}, \omega)$ shows that the energy range over which $\text{Im} \chi^0(\mathbf{q}, \omega)$ is finite initially increases as $4t'aq$, but then increases more rapidly with q , eventually overtaking the magnon energy. Therefore for short wavelength modes, the magnon energy falls within this range, resulting in the broadening.

The magnon softening is seen to be moderately q dependent. While the magnon peak shifts to nearly $\omega \approx 0$ at $x \sim 10\%$ for small q , a substantial energy gap still remains for $q \sim 1$ (see Fig. 3). This interestingly shows that the instability of the AF state with respect to transverse fluctuations in the order parameter strongly depends on the fluctuation wavelength. While the AF state becomes unstable with respect to long wavelength modes at $x = x_c$, the short wavelength modes are still positive energy modes, so that short-range AF order should survive.

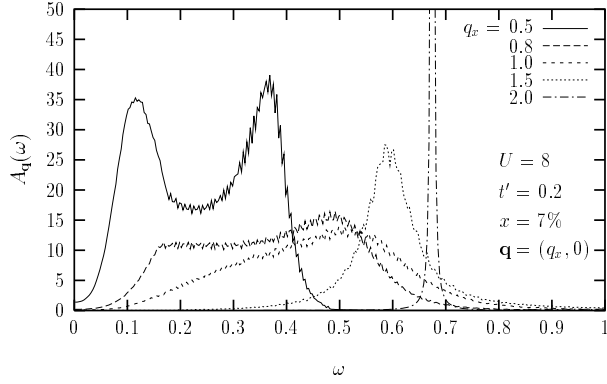


FIG. 5. The incoherent part of the magnon spectral function decreases progressively with increasing wavevector $\mathbf{q} = (q_x, 0)$, for a fixed doping concentration of $x = 7\%$. Magnon damping and linewidth sharply decrease as q_x approaches ~ 2.0 , and for $q_x \geq 2$ only the coherent magnon peak remains at low energy, with an insignificant incoherent part at higher energy (not shown).

For a fixed doping concentration, the coherent magnon peak energy is proportional to the wavevector q in the small q limit (see Fig. 4). For short wavelength modes, the incoherent part decreases dramatically with increasing wavevector (see Fig. 5). Magnon damping and linewidth sharply decrease as q approaches ~ 2.0 , and for $q \geq 2$ only the coherent magnon peak remains at low energy, with an insignificant incoherent part at higher energy.

As the doping approaches the critical concentration x_c , above which the AF state is unstable, the appearance of narrow magnon modes at very low energy despite their strong renormalization due to the intraband particle-hole excitations, is a noteworthy feature of the metallic AF state.

B. Hole doping

The strong intraband contribution renders the homogeneous AF state unstable for any amount of hole doping. [4,5] This instability with respect to transverse perturbations in the AF order is signalled by the transverse response eigenvalue $U\lambda_{\mathbf{q}}$ exceeding unity for long wavelength (small q) modes, indicating absence of long-range AF order, and signalling a tendency towards incommensurate ordering with wavevector different from $\mathbf{Q} = (\pi, \pi)$. Different types of homogeneous spiral phases, and their stability with respect to longitudinal and transverse perturbations have been studied in detail. [4]

However, short-range AF order appears stable, as indicated by the full q dependence of $U\lambda_{\mathbf{q}}$ (see Fig. 6) for the two eigenvalues $\lambda_{\mathbf{q}}$ of the $\chi^0(\mathbf{q})$ matrix for $\mathbf{q} = (q, q)$ in the range $0 < q < \pi$. The reflection symmetry about

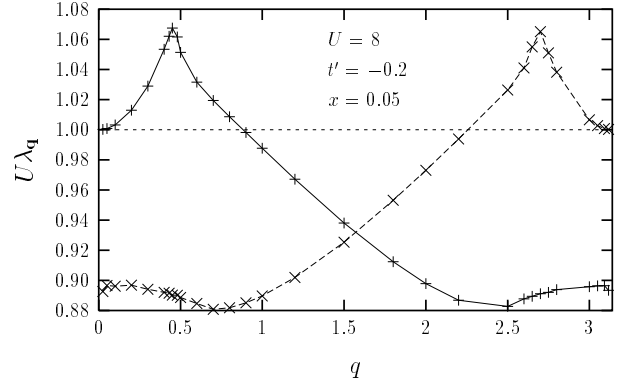


FIG. 6. The q dependence of $U\lambda_{\mathbf{q}}$ in the range $0 \leq q \leq \pi$ for the two eigenvalues $\lambda_{\mathbf{q}}$ of the $\chi^0(\mathbf{q})$ matrix for hole concentration of 5%.

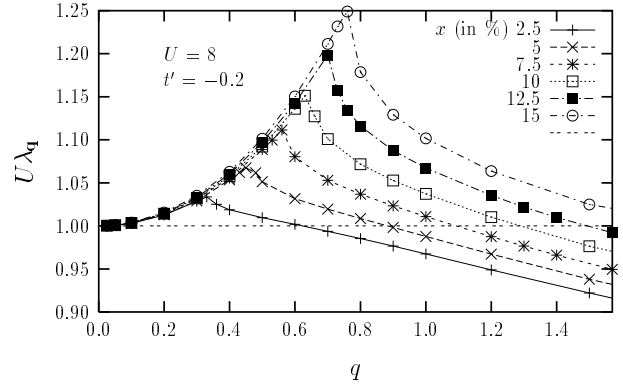


FIG. 7. The q dependence of $U\lambda_{\mathbf{q}}$ for different hole doping concentrations x , showing that $U\lambda_{\mathbf{q}}$ drops below 1 above some value $q = q^*$. Note that the small- q parabolic behaviour of $U\lambda_{\mathbf{q}}$ is independent of doping concentration.

$q = \pi/2$ is due to the location of the hole pockets around $(\pm\pi/2, \pm\pi/2)$ in the Brillouin zone. Considering the larger eigenvalue for small q , the parabolic behaviour of $U\lambda_{\mathbf{q}}$ is independent of doping concentration (see Fig. 7), as obtained earlier. [5] However, beyond a certain q value $U\lambda_{\mathbf{q}}$ starts decreasing and eventually drops below unity at $q = q^*$. This signals the stability of the AF state with respect to transverse perturbations of wavelength shorter than $\lambda^* = 2\pi/q^*$, implying that short-range AF order can exist in the hole doped AF upto length scale $\xi \sim \lambda^*$. For $x \geq 15\%$, the transverse response eigenvalue $U\lambda_{\mathbf{q}} > 1$ for all q , indicating no stability for AF domains of any size.

The q dependence of $U\lambda_{\mathbf{q}}$ for different hole doping concentrations (Fig. 7) shows that the wavevector value q^* where $U\lambda_{\mathbf{q}}$ drops below unity increases with doping concentration x , indicating diminishing spin correlation length. The behaviour of the spin correlation length $\xi/a = 2\pi/q^*$ with x is shown in Fig. 8, clearly showing a $1/\sqrt{x}$ dependence, as seen in neutron scattering

experiments. [18]

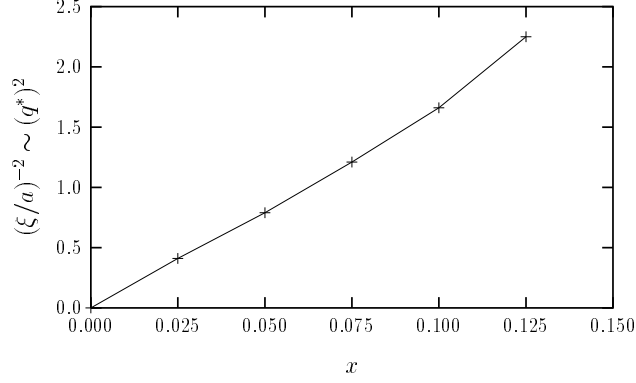


FIG. 8. Plot of $(q^*)^2$ vs. x shows a linear dependence, implying a $x^{-1/2}$ dependence of the spin correlation length ξ on hole doping concentration x .

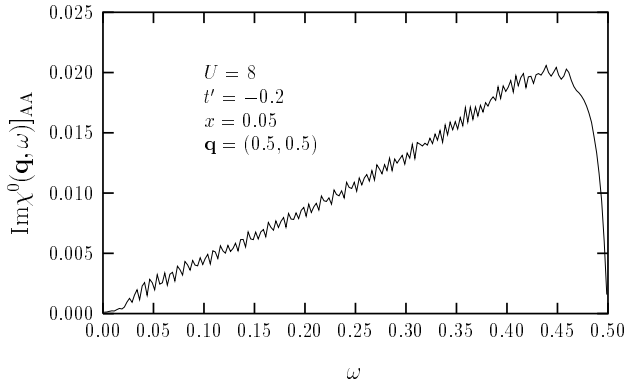


FIG. 9. The imaginary part of the particle-hole propagator $\chi^0(\mathbf{q}, \omega)$ shows a linear behaviour over a large ω range.

Figure 9 shows that imaginary part $\text{Im}[\chi^0(\mathbf{q}, \omega)]_{\text{AA}}$ on the A sublattice has a remarkably linear behaviour over a large ω range. A similar behaviour for q not too small is also observed in the electron-doped case. This low-frequency contribution in $\text{Im}\chi^0(\mathbf{q}, \omega)$, arising from the intraband excitations in the antiparallel-spin particle-hole propagator $\chi^0(\mathbf{q}, \omega)$, is suppressed to order t^2/U^2 due to the AF coherence factors. However, no such suppression is present in the parallel-spin particle-hole propagators $[\pi^0(\mathbf{q}, \omega)]_{\text{AA}}$ or $[\pi^0(\mathbf{q}, \omega)]_{\text{BB}}$, where both particle and hole amplitudes (in the lower band) are of order unity. Such parallel-spin particle-hole propagators are involved in the charge density fluctuations.

Although the AF state is unstable at the static level, the spectral function shows sharp peaks at finite frequency (see fig. 10). This is due to the change in sign of the intraband coefficient $\alpha_{\text{intra}}(\omega)$ with increasing ω , discernible from the change in curvature of the spectral function. As for the electron-doped case, the small- q magnon peaks are sharp because $\text{Im}\chi^0(\mathbf{q}, \omega)$ van-

ishes at the magnon-mode energy, whereas at higher q the magnon-mode energy lies within the energy scale over which $\text{Im}\chi^0(\mathbf{q}, \omega)$ is finite

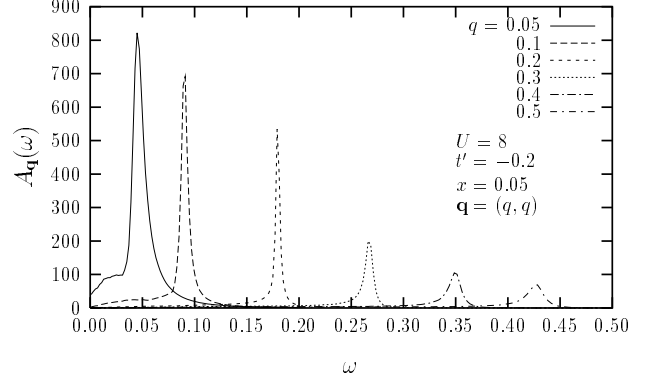


FIG. 10. The spectral function shows sharp magnon peaks for low q , and broadened peaks at higher q due to magnon damping.

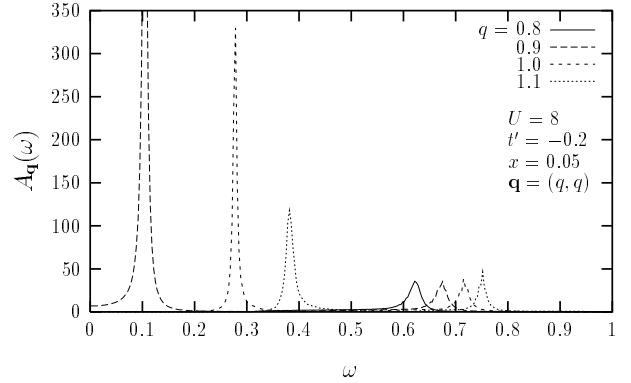


FIG. 11. For fluctuation modes of wavelength smaller than the domain size, ($q > q^* \approx 0.9$ for $x = 0.05$), the magnon modes are strongly softened, with a small incoherent part appearing at *higher* energy.

(see Fig. 9), resulting in magnon broadening.

Figure 11 shows that there is an abrupt change in the spectral function when q crosses $q^* \approx 0.9$ for $x = 0.05$ (see Figure 7). For fluctuation modes of wavelength smaller than the AF domain size ($q > q^*$), the magnon modes are strongly softened by the intraband contribution, with a small incoherent part appearing at *higher* energy. In contrast, in the electron-doped case, the coherent part was shifted to higher energy and a weak incoherent part appeared at low energy. Both magnon damping and softening have been observed in the hole-doped cuprate $\text{La}_{2-x}\text{Ba}_x\text{CuO}_4$. [19]

IV. FINITE TEMPERATURE SPIN DYNAMICS

At finite temperature $T \ll J$, the decrease in sublattice magnetization $m(T)$ due to thermal excitation of long wavelength magnons has been studied in a highly anisotropic layered antiferromagnet with planar exchange

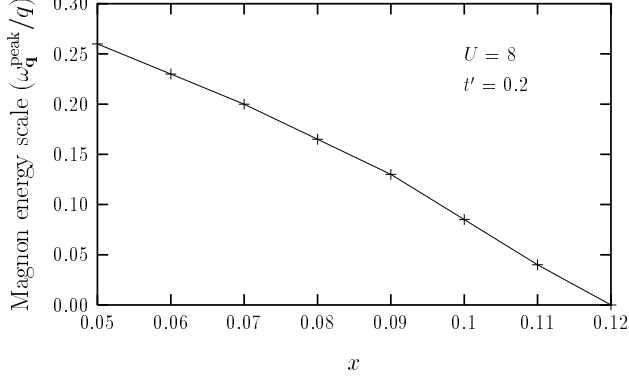


FIG. 12. The long-wavelength magnon energy scale ω_q^{peak}/q falls linearly with the doping concentration x , implying a corresponding decrease in the spin-wave stiffness constant and the Néel temperature.

interaction energy $J = 4t^2/U$, an effective interlayer hopping t_z , [20] and an effective anisotropy gap Δ_{DM} due to the Dzyaloshinski-Moriya interaction. [21] An estimate of the Néel temperature T_N was obtained from the predominant $T \ln T$ fall off of $m(T)$ with T as $k_B T_N \sim J/\ln(1/r)$ for $\Delta_{\text{DM}} \ll 2Jr$, and $k_B T_N \sim J/\ln(J/\Delta_{\text{DM}})$ for $2Jr \ll \Delta_{\text{DM}}$, where $r = t_z/t$ is the interlayer-to-planar hopping ratio. In both cases, T_N is proportional to the long wavelength magnon energy scale $(\omega_q/q)_{q \rightarrow 0} \sim J$.

Figure 2 shows that the relevant magnon energy scale which will essentially determine the low temperature spin dynamics in the doped AF is the incoherent magnon peak energy, which shifts to lower energy and gains spectral weight with increasing doping. The doping dependence of this magnon energy scale ω_q^{peak}/q shows a nearly linear decrease with doping concentration (see Fig. 12).

This nearly linear decrease in the incoherent magnon peak energy with doping concentration provides an explanation for the observed decrease in unison of the spin-wave stiffness constant ρ_s and the Néel temperature T_N with Ce doping in both $\text{Nd}_{2-x}\text{Ce}_x\text{CuO}_4$ and $\text{Pr}_{2-x}\text{Ce}_x\text{CuO}_4$. [3] A spin dilution model, within which a Cu^{2+} $S=1/2$ ion is assumed to be converted into a localized Cu^{1+} $S=0$ ion for each added Ce ion, has been found to quantitatively describe the x -dependence of ρ_s and T_N . [2] However, the localization of the added electrons in this scenario contradicts the metallic conductivity resulting from Ce doping.

V. SPIN-FLUCTUATION CORRECTION TO SUBLATTICE MAGNETIZATION

Figure 13 shows the first-order spin-fluctuation correction to the electron propagator. Physically, the process (1) (2) represents a spin- \uparrow electron in state \mathbf{k} below (above) the Fermi energy emitting a virtual magnon with momentum \mathbf{Q} and flipping into a spin- \downarrow electron in state

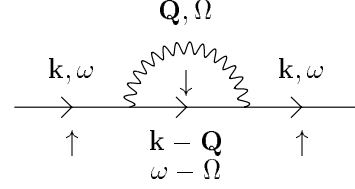


FIG. 13. The quantum spin-fluctuation correction to the electron propagator, representing a spin flip accompanied by the emission and absorption of a virtual magnon.

$\mathbf{k} - \mathbf{Q}$ above (below) the Fermi energy, which then re-absorbs the virtual magnon. Such spin-flip processes involve transfer of spectral weight across the Fermi energy, and therefore result in corrections to electron densities n_\uparrow and n_\downarrow , and hence to the sublattice magnetization.

Considering first the process (1) involving $E_{\mathbf{k}} < E_F$ and $E_{\mathbf{k}-\mathbf{Q}} > E_F$, the integrated spectral weight transferred above the Fermi energy yields the reduction in the spin- \uparrow density on an A-sublattice site

$$\begin{aligned} -\delta n_\uparrow^{(1)} &= \sum_{\mathbf{k}} \int_{E_F}^{\infty} \frac{d\omega}{\pi} \text{Im} [\delta G_\uparrow(\mathbf{k}, \omega)]_{AA} \\ &= \sum_{\mathbf{k}, \mathbf{Q}} U^2 \int \frac{d\Omega}{\pi} \text{Im} \chi_R^{-+}(\mathbf{Q}, \Omega) \frac{a_{\mathbf{k}-\mathbf{Q}, \downarrow}^2}{(E_{\mathbf{k}-\mathbf{Q}} - E_{\mathbf{k}} + \Omega)^2} \end{aligned} \quad (17)$$

involving the retarded part of the magnon propagator $\chi_R^{-+}(\mathbf{Q}, \Omega)$. Here $a_{\mathbf{k}-\mathbf{Q}, \downarrow}^2$ is the spin- \downarrow electron density on the A sublattice site, and in the strong coupling limit, is given by 1 and $\epsilon_{\mathbf{k}-\mathbf{Q}}^2/4\Delta^2$ for state $\mathbf{k} - \mathbf{Q}$ in the upper and lower band, respectively.

For the undoped antiferromagnet, where the spin-flip process involves an interband excitation, and states \mathbf{k} and $\mathbf{k} - \mathbf{Q}$ are energetically separated by the AF gap 2Δ , this correction reduces the A-sublattice density n_\uparrow from 1 to 0.8 for the square lattice. [22] A similar process transfers spin- \downarrow spectral weight from the upper (unoccupied) band to the lower band, increasing n_\downarrow from 0 to 0.2, resulting in a net reduction of 0.4 in the sublattice magnetization.

In the metallic antiferromagnet, however, spin-flip processes involve the intraband excitations as well, and the small energy denominator $E_{\mathbf{k}-\mathbf{Q}}^\ominus - E_{\mathbf{k}}^\ominus \sim 4t'Qa$ in the $Q \ll 1$ limit drastically increases the spin-fluctuation contribution to the particle density correction. On the other hand, the phase-space restriction on states \mathbf{k} and $\mathbf{k} - \mathbf{Q}$ to lie across the Fermi energy suppresses the intraband contribution in the long-wavelength limit by a

factor Q . In the following, we examine the combined effect of these two features of intraband excitations on the quantum correction to sublattice magnetization.

As discussed earlier, except for a renormalized magnon velocity c and amplitude Z , the coherent part of the magnon propagator for $Q \ll 1$ is qualitatively unchanged in the weak doping limit ($\sqrt{2}J > 4t'a$), with $\text{Im } \chi_R^{+}(\mathbf{Q}, \omega) \sim (Z/Q)\delta(\omega - cQ)$ as for the AF insulator. Substituting in Eq. (17), we obtain

$$-\delta n_{\uparrow}^{(1)} = \frac{U^2 t^2 a^4}{4\Delta^2} \int \frac{Q dQ}{2\pi} \int_{-\pi/2}^{\pi/2} \frac{ad\theta Q \cos \theta}{(2\pi)^2} \cos^2 2\theta \times \int \frac{d\Omega}{\pi} \frac{Z}{Q} \delta(\Omega - cQ) \frac{1}{(4t'aQ \cos \theta + \Omega)^2} \quad (18)$$

After doing the Ω integral, the resulting Q integral in Eq. (18) is of the form $\int dQ/Q$, which yields a logarithmically divergent reduction in the A-sublattice density n_{\uparrow} from process (1). Similarly, the process (2) involving $E_{\mathbf{k}}^{\ominus} > E_F$ and $E_{\mathbf{k}-\mathbf{q}}^{\ominus} < E_F$, and the advanced part of the magnon propagator $\chi_A^{+}(\mathbf{Q}, \Omega)$, transfers spectral weight below the Fermi energy, yielding an identical logarithmically divergent enhancement to n_{\uparrow} . Remarkably, it is this exact cancellation of two logarithmically divergent contributions which is responsible for the survival of long-range AF order in the weakly (electron) doped cuprate.

VI. CONCLUSIONS

The study of spin fluctuations in the $t - t'$ Hubbard model shows that when doped electrons (holes) are added to the bottom (top) of the upper (lower) Hubbard band, the consequent intraband particle-hole excitations strongly renormalize the magnon propagator in the metallic AF state. The change in sign of the intraband coefficient $\alpha_{\text{intra}}(\omega)$ with ω is a key result, leading to differences between static and dynamical behaviours. Several features of the magnetic properties of the electron and hole doped cuprates are understandable within this microscopic model. These include: i) finite (nearly zero) critical doping concentration x_c above which long-range AF order is destroyed in electron (hole) doped cuprates, ii) a linear decrease in the spin-wave stiffness constant and Néel temperature with doping concentration, iii) magnon broadening and softening in hole doped cuprates, iv) enhanced correlations at the dynamical level.

However, important features of the hole-doped cuprates require further investigation. While the $t - t'$ Hubbard model (with negative t') indicates instability of the AF state and tendency towards incommensurate ordering for any finite hole doping, spin fluctuations in the hole-doped cuprates are commensurate for low doping and a commensurate-incommensurate transition occurs at $x \approx 0.05$. The exact mechanism responsible for the

loss of long-range AF order for $x < 0.05$ therefore remains unclear. Interestingly, it is in this doping regime that a magnon damping term $\Gamma \sim T$ in $\text{La}_{2-x}\text{Sr}_x\text{CuO}_4$ and $\text{La}_{2-x}\text{Ba}_x\text{CuO}_4$ has been observed at finite temperature, [23,24] which accounts for the anomalous nuclear spin relaxation rate, resistivity etc.

[†] Electronic address: avinas@iitk.ac.in

- ¹ T. R. Thurston, M. Matsuda, K. Kakurai, K. Yamada, Y. Endoh, R. J. Birgeneau, P. M. Gehring, Y. Hidaka, M. A. Kastner, T. Murakami, and G. Shirane, Phys. Rev. Lett. **65**, 263 (1990).
- ² C. Almasan and M. B. Maple, in *Chemistry of High-Temperature Superconductors*, edited by C. N. R. Rao, World Scientific, Singapore (1991).
- ³ M. Matsuda, Y. Endoh, K. Yamada, H. Kojima, I. Tanaka, R. J. Birgeneau, M. A. Kastner, and G. Shirane, Phys. rev. **45**, 12548 (1992).
- ⁴ A. V. Chubukov and K. A. Musaelian, J. Phys.: Condens. Matter, **7**, 133, (1995).
- ⁵ A. Singh and H. Ghosh, Phys. Rev. B **65**, 134414 (2002).
- ⁶ R. Coldea, S. M. Hayden, G. Aeppli, T. G. Perring, C. D. Frost, T. E. Mason, S.-W. Cheong, and Z. Fisk, Phys. Rev. Lett. **86**, 5377 (2001).
- ⁷ N. M. R. Peres and M. A. N. Araújo, Phys. Rev. B **65**, 132404 (2002).
- ⁸ A. Singh and P. Goswami, Report No. cond-mat/0205117 (2002).
- ⁹ P. Bénard, L. Chen, and A. -M. S. Tremblay, Phys. Rev. B **47**, 589 (1993); A. Veilleux, A. Daré, L. Chen, Y. M. Vilks, and A. -M. S. Tremblay, Phys. Rev. B **52**, 16255 (1995).
- ¹⁰ T. Tohyama and S. Maekawa, Phys. Rev. B **49**, 3596 (1993).
- ¹¹ G. Stemmman, C. Pépin, and M. Lavagna, Phys. Rev. B **50**, 4075 (1994).
- ¹² O. K. Andersen, A. I. Liechtenstein, O. Jepsen, and F. Paulsen, J. Phys. Chem. Solids **56**, 1573 (1995).
- ¹³ Z. Z. Wang, T. R. Chien, N. P. Ong, J. M. Tarascon, and E. Wang, Phys. Rev. B **43**, 3020 (1991); S. J. Hagen, J. L. Peng, Z. Y. Li, and R. L. Greene, *ibid.* **43**, 13606 (1991); S. Kohiki, J. Kawai, T. Kamada, S. Hayashi, H. Adachi, K. Setsune, and K. Wasa, Physica C **166**, 437 (1990).
- ¹⁴ T. Sasaki *et al.*, Solid. St. Commun. **75**, 93 (1990).
- ¹⁵ S. Carter *et al.*, Phys. Rev. Lett. **67**, 3440 (1991); W. Bao *et al.*, *ibid.* **71**, 766 (1993).
- ¹⁶ S. Sudo, J. Mag. Mag. Mat. **114**, 57 (1992).
- ¹⁷ A. Singh, Report No. cond-mat/0006079 (2000).
- ¹⁸ T. R. Thurston, R. J. Birgeneau, M. A. Kastner, N. W. Preyer, G. Shirane, Y. Fujii, K. Yamada, Y. Endoh, Y. Hidaka, and T. Murakami, Phys. Rev. B **40**, 4585 (1989).
- ¹⁹ G. Aeppli, S. M. Hayden, H. A. Mook, Z. Fisk, S.-W. Cheong, D. Rytz, J. P. Remeika, G. P. Espinosa, and A. S. Cooper Phys. Rev. Lett. **62**, 2052 (1989).

- ²⁰ A. Singh, Z. Tešanović, H. Tang, G. Xiao, C. L. Chien, and J. C. Walker, Phys. Rev. Lett. **64**, 2571 (1990).
- ²¹ A. Singh and Z. Tešanović, Phys. Rev. B **43**, 11445 (1991).
- ²² A. Singh and Z. Tešanović, Phys. Rev. B **41**, 614 (1990); *ibid.* **41**, 11 457 (1990).
- ²³ S. M. Hayden, G. Aeppli, R. Osborn, A. D. Taylor, T. G. Perring, S.-W. Cheong, and Z. Fisk, Phys. Rev. Lett. **67**, 3622 (1991).
- ²⁴ B. Keimer, R. J. Birgeneau, A. Cassanho, Y. Endoh, R. W. Erwin, M. A. Kastner, and G. Shirane, Phys. Rev. Lett. **67**, 1930 (1991).